Journal of the Atmospheric Sciences

Isentropic analysis of moist convection

--Manuscript Draft--

Manuscript Number:	
Full Title:	Isentropic analysis of moist convection
Article Type:	Article
Corresponding Author:	Olivier Pauluis, Ph.D. New York University New York, NY UNITED STATES
Corresponding Author's Institution:	New York University
First Author:	Olivier Pauluis, Ph.D.
Order of Authors:	Olivier Pauluis, Ph.D.
	Agnieszka A. Mrowiec
Abstract:	In this paper the convective mass transport is analyzed by sorting air parcels in terms of their entropy and an isentropic streamfunction for convective motions is introduced. By averaging the upward mass flux at constant value of the equivalent potential temperature, one can compute an isentropic mass transport which filters out reversible oscillatory motions such as gravity waves. This novel approach emphasizes the fact that the upward energy and entropy transports by convection are due to the combination of ascending air parcels with high energy and entropy and subsiding air parcels with lower energy and entropy. The use of conditional averaging is extended to other dynamic and thermodynamic variables such as vertical velocity, temperature or relative humidity to obtain a comprehensive description of convective motions. It is also shown how this approach can be used to determine the mean diabatic tendencies from the three dimensional dynamic and thermodynamic fields. A two-stream approximation that partitions the isentropic circulation into a mean updraft and mean downdraft is also introduced. This offers a straightforward way to identify the mean properties of rising and subsiding air parcels. The results from the two-stream approximation are compared with two other definitions of the cloud mass flux. It is argued that the isentropic analysis offers a robust definition of the convective mass transport that is not tainted by either the choice of an arbitrary threshold for vertical velocity or condensate content, and that separates the irreversible convective overturning from oscillations associated with gravity waves.
Suggested Reviewers:	

Page and Color Charge Estimate Form

Click here to download Page and Color Charge Estimate Form: Page_Charge_Estimation_Form-2.pdf

Isentropic analysis of convective motions

Olivier M. Pauluis *

Center for Atmosphere Ocean Science Courant Institute of Mathematical Sciences New York University

Agnieszka A. Mrowiec

Columbia University / NASA Goddard Institute for Space Studies

* *Corresponding author E-mail:* pauluis@cims.nyu.edu

ABSTRACT

In this paper the convective mass transport is analyzed by sorting air parcels in terms of their entropy and an isentropic streamfunction for convective motions is introduced. By averaging the upward mass flux at constant value of the equivalent potential temperature, one can compute an isentropic mass transport which filters out reversible oscillatory motions such as gravity waves. This novel approach emphasizes the fact that the upward energy and entropy transports by convection are due to the combination of ascending air parcels with high energy and entropy and subsiding air parcels with lower energy and entropy. The use of conditional averaging is extended to other dynamic and thermodynamic variables such as vertical velocity, temperature or relative humidity to obtain a comprehensive description of convective motions. It is also shown how this approach can be used to determine the mean diabatic tendencies from the three dimensional dynamic and thermodynamic fields.

A two-stream approximation that partitions the isentropic circulation into a mean updraft and mean downdraft is also introduced. This offers a straightforward way to identify the mean properties of rising and subsiding air parcels. The results from the two-stream approximation are compared with two other definitions of the cloud mass flux. It is argued that the isentropic analysis offers a robust definition of the convective mass transport that is not tainted by either the choice of an arbitrary threshold for vertical velocity or condensate content, and that separates the irreversible convective overturning from oscillations associated with gravity waves.

1. Introduction

Atmospheric convection transports energy and water from the Earth's surface to the free troposphere. The ascent of warm, moist air in saturated turbulent plumes is balanced by subsidence of dryer and colder air that takes place in the environment or in convective or mesoscale downdrafts. Convective systems however rarely occur as simple overturning motions; rather they are associated with a variety of turbulent motions over a wide range of scales. Any analysis of such flow is complex as individual air parcels undergo multiple dynamical and thermodynamical transformations. For example, one may want to separate of irreversible ascent and mixing of air parcels from the gravity waves. However, such separation is not straightforward as convective plumes originating from the boundary layer and gravity waves are often spatially and temporally collocated. The main purpose of this paper is to introduce a new technique to diagnose the convective overturning in numerical models.

The proposed approach takes advantage of the quasi-conservation of entropy to isolate convective motions from oscillatory motions. In practice, this amounts to averaging various aspects of the flow in isentropic coordinates. Isentropic analyses have been widely used to study the large-scale atmospheric and oceanic circulation (Dutton 1976; Johnson 1989; Held and Schneider 1999; Pauluis et al. 2008, 2010), but have not yet been applied to study convective motions. As the entropy of an air parcel is conserved for reversible adiabatic motions, it is expected remain almost constant for time significantly longer than the convective drafts, even as air parcels may experience large changes in pressure or temperature. Therefore, by averaging the circulation on isentropic surfaces the same set of parcels may be followed, and thus a better approximation of the Lagrangian trajectories of the air parcels may be obtained. While this argument has traditionally been applied to separate the large-scale planetary circulation from synoptic scale eddies, it is shown here that it offers a straightforward way to separate irreversible overturning by convective motions from reversible oscillations by gravity waves.

Section 2 introduces the isentropic averaging for the convective mass transport and defines the convective streamfunction. An isentropic upward mass transport is obtained by sorting the upward mass transport at each level in terms of its equivalent potential temperature. This mass transport can then be integrated to obtain the stream function, which offers a simpler representation of the convective circulation. This methodology is used to analyze radiative convective equilibrium simulations with the System for Atmospheric Modeling (SAM, Khairoutdinov and Randall 2003). In Section 3, the isentropic averaging is generalized to assess the thermodynamic and dynamical properties of the air parcels. It can be used to define the probability of occurrence, mean vertical velocity, and mean thermodynamic properties such as water content and buoyancy of air parcels in terms of of heigh and equivalent potential temperature. Thus it is possible, for example, to isolate a population of intense, almost undiluted updrafts associated with peak vertical velocities of bout 40 ms^{-1} in numerical simulations. Section 4 shows application of the isentropic analysis to determine the mean diabatic tendency from the convective stream function. Furthermore, an empirical entrainment and an entrainment scale height can be determined as functions of equivalent potential temperature and height. Section 5 introduces a two-stream decomposition of the convective motions based on the isentropic analysis. The convective circulation is partitioned between mean upward and mean downward flows of equal mass transport but different thermodynamic properties. These results are contrasted with two other definitions of the convective mass transport. It is shown here, that the isentropic analysis leads to significantly lower value of the convective mass transport particularly in the upper troposphere.

2. Isentropic streamfunction

The isentropic averaging technique discussed below will be applied to analyze a simulation of radiative-convective equilibrium performed with the System for Atmospheric Modeling (SAM), a Cloud Resolving Model developed by Khairoutdinov and Randall (2003). The model was integrated on 216 km x 216 km x 28 km domain at 500 m horizontal resolution and stretched vertical grid with 64 gridpoints, with periodic boundary conditions in the horizontal directions. The lower boundary is an ocean surface at constant temperature of 301 K, while a sponge layer is applied in the upper 8 km to prevent the reflection of gravity waves. The model uses a 5 species single-moment microphysics, an explicit radiative transfer, and was integrated for 100 days, with the last 60 days used for the time averaging.

We introduce the time and horizontal mean isentropic value of a given variable f as:

$$\langle f \rangle (z, \theta_{e0}) = \frac{1}{P L_x L_y} \int_0^P \int_0^{L_y} \int_0^{L_x} f(x,y,z,t) \delta(\theta_{e0} - \theta_e(x,y,z,t)) dx\, dy\, dt. \qquad (1)$$

Here, ρ is the mass per unit volume, θ_e is the equivalent potential temperature, P is the time period over which the averaging is performed, and L_x and L_y are the horizontal extent of the domain. The integral in eqn. 1 involves a Dirac delta function $\delta(\theta_{e0} - \theta_e(x,y,z,t))$, which is approximated here by a function that is equal to $1/\Delta\theta_e$ between $\theta_e - 0.5\Delta\theta_e$ and $\theta_e + 0.5\Delta\theta_e$, and 0 elsewhere. In practice, this amount to sorting the air parcels in terms of the equivalent potential temperature and to summing the quantity f at each level in finite θ_e bins. The mean isentropic value, as defined here, is therefore a function of height, time and equivalent potential temperature. In addition, for simplicity of notation, the dependency on (z, θ_e) will be not be explicitly indicated from now on, but it should be understood that all the mean isentropic values $\langle \cdot \rangle$ are function of both z and θ_e.

The isentropic mean distribution of $\langle \rho w \rangle$ in the radiative-convective equilibrium simulation is shown in Figure 1a. The solid black line shows the horizontal mean profile of equivalent potential temperature $\overline{\theta}_e(z)$. The quantity $\langle \rho w \rangle$ is referred to as the isentropic upward mass flux distribution, in units of (kg m^{-2} s^{-1}K $^{-1}$), corresponding to an upward mass flux per unit of equivalent potential temperature. The quantity $\langle \rho w \rangle \, \delta\theta_e$ corresponds to the net upward mass flux of air parcels at level z with an equivalent potential temperature between θ_e and $\theta_e + \delta\theta_e$. The mass flux distribution can be used to define an isentropic streamfunction as:

$$\Psi(z, \theta_e) = \int_{-\infty}^{\theta_e} \langle \rho w \rangle \, (z, \theta_e') d\theta_e'. \tag{2}$$

The isentropic streamfunction is shown in Figure 1b. The streamfunction is negative through most of the atmosphere, corresponding to an upward entropy transport. The absolute minimum of the streamfunction is located near the surface and is associated with mixing within the sub-cloud layer. The magnitude of the streamfunction decreases sharply above 1km. Ascending air parcels originating from the lowest atmospheric layer have high values of θ_e, up to 355 K. The equivalent potential temperature drops rapidly with height indicating entrainment of dryer air in the updrafts. Above 4–5 km the streamlines become almost vertical, indicating that the role of entrainment is limited above the freezing level, and that air parcels approximately conserve their equivalent potential temperature as they rise. As adiabatic freezing or sublimation can lead to an increase in the equivalent potential temperature, the apparent conservation of θ_e along the streamlines above the freezing level might actually be the results of the compensation between freezing and entrainment. Most of the detrainment occurs below 11km. The streamfunction changes sign at about 12 km, indicating presence of convective overshoots associated with the net weak downward entropy transport as low entropy air rises and mixes with higher entropy air from above before subsiding.

In the upper troposphere, the equivalent potential temperature of subsiding air decreases as the parcels move downward because of radiative cooling. The bulk of the downward motion is centered around the mean atmospheric state (see Figure 1). At a height of approximately 4.5 km, there is a sharp drop in the θ_e of the downward flow, associated with the melting of precipitation (melting of ice reduces the θ_e in the air parcel). The minimum θ_e value of about 320 K occurs at this level and is associated with an increase in the downward mass flux. Below the freezing level, the equivalent potential temperature of subsiding air parcels gradually increases as they approach the surface. While radiative cooling is still active in these regions, the increase of θ_e is directly tied to the mixing between subsiding environmental air and detraining cloudy air with a higher value of θ_e.

3. Isentropic averaging of convective motions

The isentropic averaging (1) is not limited to upward motion. The same formalism can be applied to any variable of interest to obtain a more detailed analysis of the typical properties of the air parcels involved in convective motions. The probability density function for a parcel with equivalent potential temperature θ_e at level z can be estimated as

$$PDF(z, \theta_e) = \frac{\langle \rho \rangle (z, \theta_e, t)}{\overline{\rho}(z)} \tag{3}$$

where $\overline{\rho}(z)$ is the horizontal mean density. The logarithm of the frequency of occurrence is shown on the left panel of Figure 2. The maximum probability is centered around the mean profile in the mid troposphere, corresponding to subsiding air parcels already noted in Figure 1. Interestingly, the upper end of the frequency distribution follows closely a line of constant value of θ_e, which indicates that undiluted air parcels from the boundary layer can be found through the entire troposphere, although they are very scarce (with a probability density less 10^{-4} K^{-1}) and do not contribute significantly to the total upward mass transport. Similarly, the presence of low θ_e air parcels that extends from the mid tropospheric θ_e minimum at 5 km down to the top of the mixed layer can be observed. The presence of a fair number of parcels with θ_e of $330K$ or less, which is significantly less than the mean profile minimum value of about $331K$, should also be pointed out. Near the surface, the low tail of the equivalent potential temperature distribution is limited to relatively high value of θ_e. The probability of finding a parcel with θ_e less than 338 K in the boundary layer is approximately 0.0004, while the mean profile reaches the same potential temperature at a height of 1000m. This indicates that the downdrafts that reach the surface originate mostly from within the planetary boundary layer the boundary layer, and not from the mid-tropospheric minimum of θ_e.

The mean mass flux $\langle \rho w \rangle$ and the mean isentropic density $\langle \rho \rangle$ can be combined to define the mean vertical velocity for a parcel at a given value of θ_e at level z:

$$\tilde{w}(z, \theta_e) = \frac{\langle \rho w \rangle (z, \theta_e)}{\langle \rho \rangle (z, \theta_e)} \tag{4}$$

The mean vertical velocity, shown on the right-hand (Figure 2b), exhibits a significant asymmetry between fast upward ascent at high θ_e and very slow subsidence at value of θ_e corresponding to the horizontal mean value, and is in good agreement with the conceptual model of Bjerkness (1938). The high values of $\tilde{w}$ (up to 40 m s^{-1}) observed in the upper troposphere at high θ_e correspond to a very strong, rare, weakly diluted or undiluted updrafts. The abrupt decrease of high $\tilde{w}$ at 12km does not necessarily means that these strong updrafts are blocked at that level. Rather, due to the density averaging in the definition of $\tilde{w}$ (equation 4), the value of $\tilde{w}$ decreases near the mean profile as fast rising parcels have the same potential temperature as a much larger number of slow moving parcels in the environment. Analysis of higher moments of the distribution could be used to further investigate the overshoot of these strong updrafts above their level of neutral buoyancy. Interestingly, while the isentropic analysis did detect strong updraft associated with high value of θ_e, there is little indication of strong downward motion at low value of θ_e that would correspond to strong convective downdrafts.

The averaging procedure used to define the mean vertical velocity of air parcel at a given height and equivalent potential temperature can be applied to any variable. We define the mass weighted isentropic average for f as

$$\tilde{f}(z, \theta_e) = \frac{< \rho f >}{< \rho >}. \tag{5}$$

This formulation allows us to define the thermodynamic properties of the air parcels as they rise or descent in the atmosphere. Figure 3 shows the mean value of the temperature $\tilde{T}$ (a), specific humidity $\tilde{q}$ (b), condensed water content $\tilde{q}_l + \tilde{q}_i$ (c) and buoyancy $\tilde{B}$ (d). The temperature decreases with height until its minimum near the tropopause at about 16 km. The coldest temperature can be associated with overshoots from the deep convective towers at around 15 km. There is a weak inflection line visible in the temperature distribution in the angle made by the isotherms (Figure 3a). A similar inflection line is also present in the humidity distribution for the same value of z and θ_e. The inflection marks the separation between unsaturated parcels to the left of the line and saturated parcels to the right. In fact, as discussed in Stevens (2005); Pauluis et al. (2008), the saturation of air parcels is characterized by a discontinuity in the equation of state. This means, for example, that the partial derivative

$$\left(\frac{\partial T}{\partial \theta_e} \right)_{p, q_T}$$

has a different value depending on whether a parcel is saturated or not. This is confirmed by the distribution of $\tilde{q}_l + \tilde{q}_i$ (Figure 3c), which shows that the inflection lines in the distributions of $\tilde{T}$ and $\tilde{q}$ indeed correspond to appearance of condensate. [1]

[1] The quantities $\tilde{T}$ and $\tilde{q}_v$ are obtained by averaging over both saturated and unsaturated parcels. Therefore, they need not to exhibit a strict discontinuity in their partial derivative. The fact that one is apparent in Figure 3 indicates that saturated and unsaturated air parcels can be fairly well separated by their value of θ_e at a given level.

4. Diabatic tendency

For a system in statistical equilibrium, the continuity equation can be written as

$$\frac{\partial}{\partial z}\left\langle \rho w \right\rangle + \frac{\partial}{\partial \theta_e}\left\langle \rho \dot{\theta}_e \right\rangle = 0. \tag{6}$$

The second term on the left-hand side corresponds to mass weighted average of the diabatic tendency $\dot{\theta}_e$. Equation 6 combined with the definition 2 makes it possible to express the diabatic tendency in terms of the vertical derivative of the stream function:

$$\left\langle \rho \dot{\theta}_e \right\rangle = -\frac{\partial \Psi}{\partial z}. \tag{7}$$

The mass weighted diabatic heating $\left\langle \rho \dot{\theta}_e \right\rangle$ is shown in Figure 4. Large heating rates are found near the surface corresponding to the surface latent and sensible heat fluxes. In the lower troposphere, a dipole of positive tendency at lower θ_e and negative tendency at higher θ_e is a result of diffusion of water vapor from moist updrafts to the dryer environment. The upper troposphere is dominated by the negative tendencies associated with radiative cooling. Parcels along the θ_e profile (solid black line) experience a net cooling due to radiation in the upper troposphere, but by a net heating in the lower troposphere as unsaturated air parcels in the environment gain more energy from diffusion of water vapor than they lose from the emission of infrared radiation.

Alternatively, the isentropic mean diabatic tendency can also be expressed as

$$\tilde{\dot{\theta}}_e = \frac{\left\langle \rho \dot{\theta}_e \right\rangle}{\left\langle \rho \right\rangle},$$

and is shown in Figure 4b. Large negative values of the diabatic tendency (on the order of 1000 K day^{-1}, are associated with the diffusion of water vapor out of cloudy air parcels. This contrasts with a much slower rate of increase in θ_e associated with the moistening of dry air, as the water vapor flux is diffused into a much larger mass of environmental air.

The equivalent potential temperature in updrafts increases between 4 and 8 km due to the freezing of liquid water and condensation of water vapor on ice crystals.

The distribution of diabatic heating can be used in a simple model to determine the entrainment rate in ascending air parcels. Neglecting the effects of radiative cooling, allows to approximate the potential temperature tendency in the updrafts by:

$$\frac{d\theta_e}{dt} = \frac{\overline{\theta}_e - \theta_e}{\tau_e}, \tag{8}$$

where τ_e corresponds to the time it takes to entrain environmental air into an updraft. This time-scale can be estimated based on the isentropic analysis as:

$$\tau_e(z, \theta_e) = \frac{\overline{\theta}_e - \theta_e}{\tilde{\dot{\theta}}_e}. \tag{9}$$

The product of the entrainment time-scale and the vertical velocity can then be expressed in terms of an entrainment scale-height λ_e,

$$\lambda_e(z, \theta_e) = \frac{\tilde{w}(\overline{\theta}_e - \theta_e)}{\tilde{\dot{\theta}}_e}. \tag{10}$$

The entrainment rate and scale-height for the radiative-convective equilibrium simulations are shown in Figure 4c and 4d.

Kuang and Bretherton (2006) similarly use equation (8) to assess the effect of entrainment. However, in their approach, one must first assume a given value of the entrainment rate to determine the value of the equivalent potential temperature following an air parcel at various height. In contrast, here we use the results from the isentropic analysis to determine the mean rate of change of the equivalent potential temperature, which is then used to determine effective entrainment rate associated with various parcels. From a geometric point of view, the quantity

$$\frac{\tilde{w}}{\tilde{\dot{\theta}}_e} = \frac{< \rho w >}{< \rho \dot{\theta}_e >} = \frac{\frac{\partial \Psi}{\partial \theta_e}}{\frac{\partial \Psi}{\partial z}}.$$

is the slope of a streamline determined form the isentropic analysis in Figure 1b. The entrainment scale height is obtained by normalizing this slope by the distance to the mean profile $\overline{\theta_e}(z)$. When the streamlines are almost vertical, the entrainment scale height is large, and there is little or no entrainment. Conversely, when the streamlines are close to horizontal, the entrainment scale height is small, corresponding to strongly entraining plumes. It should also be stressed that equation 8 does not account for the effect of freezing, which can lead to an increase in the equivalent potential temperature, and the definition of the entrainment time-scale and scale-height should not be applied below the freezing point of water.

These diagnostics for the entrainment shown in Figure 4c and 4d reveal a very large amount of mixing within the sub-cloud layer, which is associated with a large number of the shallow overturning eddies that do not rise above 1km. The mixing height there can be on the order of 500m or less, which corresponds to the model resolution. In contrast, in the free troposphere, the distribution of mixing scale height varies from relative short, one km or less for parcels founds near the mean profile to value of several kilometers at large value of θ_e typical of the sub-cloud layer. This indicates that updrafts with high values of θ_e indeed correspond to almost undiluted air parcels but are quite scarce, while the bulk of the ascending air is associated with weaker but more strongly entraining updrafts.

5. Mass flux and entrainment from two-stream approximation

The isentropic analysis discussed in previous section offers an efficient way to characterize the thermodynamic properties of convective updrafts and downdrafts. A two stream approximation is introduced here to synthesize this information more succinctly. The convective overturning is divided into a mean updraft and a mean downdraft based on the convective stream function. First, we define the upward and downward mass transports M^+ and M^-:

$$M^+(z) = \int_{-\infty}^{\infty} < \rho w > H(< \rho w >) d\theta_e \tag{11}$$

$$M^-(z) = \int_{-\infty}^{\infty} < \rho w > H(- < \rho w >) d\theta_e, \tag{12}$$

where H is a Heaviside step function. Note that if the net mass transport vanishes, mass transports in the mean updraft and downdraft cancel each other out in the absence of mean vertical motion: $M^+ + M^- = 0$. Therefore, the updraft mass transport is given by the amplitude of the streamfunction, i.e.

$$M^+(z) = \max_{\theta_e}(\Psi) - \min_{\theta_e}(\Psi). \tag{13}$$

It is common to analyze the convective circulation in terms of the upward mass transport in cloudy air columns M_{cld} and in convective cores M_{cor}, which are defined respectively as:

$$M_{\text{cld}}(z) = \frac{1}{P L_x L_y} \int_o^P \int_0^{L_y} \int_0^{L_x} w(x, y, z, t) H(q_c - \epsilon) dx\, dy\, dt \tag{14a}$$

$$M_{\text{cor}}(z) = \frac{1}{P L_x L_y} \int_o^P \int_0^{L_y} \int_0^{L_x} w(x, y, z, t) H(q_c - \epsilon) H(w - 1) dx\, dy\, dt, \tag{14b}$$

where q_c is a mass mixing ratio of cloud water, $\epsilon = 10^{-10}$ (g kg^{-1}) is a small threshold used for determining the presence of cloud water, and cores are defined with a threshold on vertical velocity: $|w| \geq 1$ m s^{-1}. The vertical profile for the mass flux M^+ from the two-stream approximation is contrasted with M_{cld} and M_{cor} in Figure (5)a. The mass flux M^+ associated with the shallow unsaturated overturning is the largest in the sub-cloud layer. The cloud base acts as a lid that reduces the net convective mass flux by more than one half. Above the cloud base, the mass flux gradually weakens all the way to a level of approximately 14km.

A major difference between the mass fluxes in clouds, convective cores, and that obtained from the isentropic analysis lies in the presence of a secondary maximum in the upward mass fluxes M_{cor} and M_{cld} in the upper troposphere (at about 12km), while the isentropic mass flux shows a monotonic decrease of the mass transport in this region. The difference is likely due to the way that the different computation of the mass transport handle oscillatory motions associated with gravity waves. The conditional averaging on vertical velocity used in the definition of the core mass flux is such that any sufficiently strong gravity wave propagating through an anvil clouds will result in a net contribution to $M_{\rm cor}$. Similarly, if a saturated air parcel overshoots its level of neutral buoyancy and then falls down after having lost its condensed water through either re-evaporation or precipitation, it will lead to a net contribution to $M_{\rm cld}$. In contrast, such oscillatory motions are not associated with any net upward isentropic transport [2]. The presence of the upper tropospheric maximum in both $M_{\rm cld}$ and $M_{\rm cor}$ but not in M^+ is a result of a rapid vertical oscillations, on time-scales corresponding either to the Brunt-Vaisala frequency, or the time-scale of cloud ice conversion into falling snow, neither of which is not directly tied with a net energy or entropy transport.

Additional information on the nature of the overturning circulation can be extracted by determining the various thermodynamic properties of the flow. For a given variable f, we define its value in the mean updraft f^+ and in the mean downdraft f^- as

$$f^+(z) = \frac{1}{M^+}\int_{-\infty}^{\infty} < \rho w f > H(< \rho w >) d\theta'_e, \tag{15a}$$

$$f^-(z) = \frac{1}{M^-}\int_{-\infty}^{\infty} < \rho w f > H(- < \rho w >) d\theta'_e. \tag{15b}$$

The transport of a quantity f by the mean updraft F_f^+ and by the mean downdraft F_f^- can then be written as:

$$F_f^+ = M^+(f^+(z) - \overline{f}(z)) \tag{16a}$$

$$F_f^- = M^-(f^-(z) - \overline{f}(z)) \tag{16b}$$

Note that in this definition, it is assumed that the upward or downward mass fluxes are compensated by a equal but opposite flux occurring at the horizontal mean value $\overline{f}$.

[2]The vertical velocity field of a gravity wave is out of phase with the equivalent potential temperature perturbation.

We first apply these definition to the moist static energy:

$$H_m = C_p T + gZ + L_v q - L_f q_i, \tag{17}$$

with C_p being heat capacity at constant pressure, T is air temperature, L_v and L_f are, respectively, the latent heat of vaporization and fusion, and q and q_i are mass mixing ratios of water vapor and ice content respectively. The mean updraft H_m^+, the mean downdraft H_m^-, and its horizontal mean value $\overline{H_m}$ are shown in Figure 5b.

While below 10 km, the mean updraft has a higher moist static energy than the mean downdraft, corresponding to an upward energy transport, above 10 km, the moist static energy of the rising air H_m^+ is less than that of the subsiding air H_m^-. Convection transports energy downwards in this region, acting as a reverse heat engine and consuming kinetic energy to transport dense, cold air upward and light, warm air downward. This can be verified by looking at the mean updraft B^+ and mean downdraft B^- buoyancies, as shown in Figure 5c. The buoyancy in the mean updraft is larger than the buoyancy in the mean downdraft between the surface and 10 km, which corresponds to a net generation of kinetic energy by the convective motions. The opposite happens above 14 km, where energy is being consumed. The definition of moist static energy (equation 17) includes latent heat of fusion, thus the presence of falling snow and ice causes a net upward energy flux, which may balance in part the downward convective energy transport in the upper troposphere.

The moist static energy in the mean downdraft is always very close to the horizontal mean, which is consistent with the fact that the mean downdraft is in large part associated with subsiding air in the unsaturated environment. However, a closer examination indicates that the moist static energy in the mean downdraft is slightly higher than the horizontal mean value everywhere except near the surface. This can be explained by the fact that a mixture between environmental and cloudy air of the same density is more dense than either air masses but has a higher moist static energy than the environment (Emanuel 1994). Thus one would expect such mixture to experience stronger downward motion, resulting in H_m^- to be slightly larger than the horizontal mean moist static energy. While the effect here is small (with $H_m^- - \overline{H_m} < 0.5$ kJ kg^{-1}), such behavior indicates that the convective energy transport cannot be accurately represented by a simple gaussian distribution around a mean atmospheric state.

The two-stream approximation can be used to determine the bulk entrainment and detrainment rate associated with the mean updraft. It is assumed that the mass flux in the mean updraft increases or decreases with height depending on the balance between entrainment and detrainment. At the same time the moist static energy in the updraft is diluted by the entrainment of environmental air. This means that the mass flux M^+ and moist static energy H_m^+ in the mean updraft are governed by the following equations:

$$\frac{dM^+}{dz} = (E - D)M^+ \tag{18}$$

$$\frac{d(M^+ H_m^+)}{dz} = EM^+\overline{H_m} - DM^+H_m^+ + L_f P_{\text{ice}}, \tag{19}$$

where E and D are the fractional entrainment and detrainment rates (per meter) respectively, L_f is the latent heat of fusion, and P_{ice} is the rate at which ice is removed by precipitation. If the vertical profiles of M^+ and H_m^+ are known, the above equations can be solved for entrainment and detrainment rates:

$$E = \frac{\frac{dH_m^+}{dz}}{\overline{H_m} - H_m^+} - \frac{L_f P_{\text{ice}}}{M^+} \tag{20}$$

$$D = E - \frac{1}{M^+}\frac{dM^+}{dz} \tag{21}$$

Note that equation 20 may yield negative value for the entrainment rate if the moist static energy in the mean updraft increases with height, which can happen in the upper troposphere. This is a limitation of the simplified model (equations 18 and 19) which considers a single rising plume to account for all convective motions. As can be seen in Figure 1, the detrainment in the upper troposphere is associated preferentially with air parcels that have lower values of θ_e than the mean updraft (and hence a lower moist static energy). Nevertheless, the results from this simple model appear reasonable in the lower 8-10km of the atmosphere and are shown in Figure 5d. The detrainment rate peaks at the cloud base, decreases with height, and is always higher than the entrainment rate, consistent with the mean updraft mass flux decreasing with height. The entrainment rate varies from 6x10^{-4} m^{-1} right above the cloud base about 2x10^{-4} m^{-1} at 8km. This indicates that while there is a vigorous entrainment in the lower troposphere, the updrafts become gradually less entraining as they rise.

6. Discussion

In this paper, a new method of analysis for convective motions in high resolution simulations has been proposed. This approach relies on conditional averaging of the various properties of air parcels in terms of both the height and the equivalent potential temperature. This averaging procedure reduces a four dimensional datasets into a two-dimensional distribution, and offers a practical way to analyze convective overturning. A conditional averaging based on equivalent potential temperature has the advantage of preserving the separation between the ascent of warm, moist air and subsidence of colder, dryer air that is a fundamental aspect of moist convection. Furthermore, as equivalent potential temperature is an adiabatic invariant of the flow, and the conditional averaging can be viewed as filtering out fast oscillatory motions such as gravity waves.

The conditional averaging has been first used here to extract a vertical mass flux, and to compute an isentropic stream function. Analysis of the streamfunction identifies the convective overturning as a combination of ascents of high energy air parcels and descent of air with much lower energy, shows the role of entrainment in reducing the equivalent potential temperature of the rising air parcels in the lower troposphere, and indicates the presence of convective overshoot in the tropopause region. There is a strong asymmetry between updrafts and downdrafts, with the former occupying a small area but occurring at fairly large vertical velocity, and the latter which are associated with slow subsidence over the large portion domain (Houze 1993). Very strong updrafts, with vertical velocities reaching 30 m s^{-1} corresponding to a rare occurrence of almost undiluted air parcels ascending from the boundary layer, were also observed. The scarcity of undulate updraft is in agreement with the recent findings of Romps and Kuang (2010). Other important properties of rising and subsiding parcels, such as temperature, humidity and buoyancy, can also be systematically recovered with the isentropic averaging approach.

Diabatic tendencies can be computed using the average value for the rate of change of the equivalent potential temperature from the continuity equation expressed in the $z - \theta_e$ coordinates. This makes it possible to retrieve diabatic tendencies from complex numerical simulations without the need for complex diagnostics within a model. When applied to the radiative-convective equilibrium simulations, our analysis shows that entrainment reduces the equivalent potential temperature in the updrafts (especially in the lower troposphere), while detrainment increases the equivalent potential temperature in subsiding air parcels. Near the freezing level a slight increase in the equivalent potential temperature of the updrafts was also found. This effect can be explained by the freezing of condensed water. Empirical entrainment rate can also be determined as a function of both height and the equivalent potential temperature. This analysis confirm the presence of significant entrainment in the lower troposphere, while the rare occurrence of updrafts with high values of θ_e correspond to air parcels that have experienced little to no entrainment.

While one of the main motivations for the isentropic averaging is to obtain a statistical description of convective motions by separating air parcels in terms of their equivalent potential temperature, it is also possible to further synthesize the information in terms of a two-stream approximation. This method defines a mean updraft and a mean downdraft based on the isentropic stream function. In doing so, one can describe a convective mass transport as well as the mean updrafts and downdrafts properties. Results from the two-stream approximation have been compared with standard definitions of the mass transport inside clouds and inside convective cores. It is shown that the isentropic analysis leads to systematically lower values for the mass transport due to the fact that the isentropic analysis filters out gravity waves (as along as these correspond to reversible oscillations of air parcels around their level neutral buoyancy), while other averaging techniques tend to include all the vertical motions.

The technique proposed here can be regarded as an equivalent of the analysis of the meridional circulation in isentropic coordinates (Dutton 1976; Johnson 1989; Held and Schneider 1999; Pauluis et al. 2008, 2010) applied to the vertical transport by convection. As convective motions act to continuously stretch and fold isentropic surfaces, their geometry is very complex in the convection. The use of the isentropic averaging can be viewed as a useful mathematical tool to disentangle this complex geometry. The isentropic averaging also serves as a quasi-Lagrangian coordinate system that filters out fast reversible oscillations and captures the core convective processes associated with high entropy updrafts balanced by slow subsidence of of low entropy air. The approach presented here is well suited for analysis of simulated convection. In addition to reduction of complex four dimensional datasets into more manageable two dimensional distributions, the isentropic analysis offers the possibility of recovering the diabatic tendencies without requiring detailed knowledge of the numerical models. This can be advantageous as one tries to diagnose the convective transport in increasingly complex numerical models in which the diabatic tendencies result from an array of physical parameterizations, including turbulent closure, microphysics, and radiative transfer. In addition, while direct computation of the isentropic stream function requires a significant amount of data, it might be possible to approximate it accurately on the basis of some statistical approximation, similarly as it can be done using the Statistical Transformed Eulerian-Mean circulation to reconstruct the global isentropic circulation (Pauluis et al. 2011). Hence, the isentropic stream function could potentially be used as an intermediary diagnostic for comparison between high resolution cloud resolving models and single column models.

Finally, a potential application of the isentropic averaging lies in the reconstruction of the transformations that various air parcels undergo as they are being transported within the convective systems. In fact, the isentropic averaging can recover not only the convective mass transport, but also the various thermodynamic properties. It is thus possible to use this information to at least approximate the thermodynamic evolution of air parcels. We plan to investigate such technique in an upcoming paper.

Acknowledgments.

This work was supported by the NSF under Grant AGS-0944058. Mrowiec's contribution to this research was supported by the DOE Office of Science, Office of Biological and Environmental Research, through contracts DE-PS02-09ER09-01 (Mrowiec) within the scope of the FASTER Project.

REFERENCES

Bjerkness, J., 1938: Saturated-adiabatic ascent of air through dry-adiabatically descending environment. *Quart. J. Roy. Meteor. Soc.*, **64**, 325–330.

Dutton, J., 1976: *The Ceaseless Wind*. McGraw-Hill, New York, 579 pp.

Emanuel, K. A., 1994: *Atmospheric Convection*. Oxford University Press, 580 pp.

Held, I. M. and T. Schneider, 1999: The surface branch of the zonally averaged mass transport circulation in the troposphere. *J. Atmos. Sci.*, **56**, 1688–1697.

Houze, R., 1993: *Cloud Dynamics*. San Diego: Academic, 573 pp.

Johnson, D. R., 1989: The forcing and maintenance of global monsoonal circulations: An isentropic analysis. *Advances in Geophysics*, **31**, 43–304.

Khairoutdinov, M. F. and D. A. Randall, 2003: Cloud resolving modeling of the ARM summer 1997 IOP: Model formulation, results, uncertainties, and sensitivities. *J. Atmos. Sci.*, **60 (4)**, 607–625.

Kuang, Z. and C. Bretherton, 2006: A mass-flux scheme view of a high-resolution simulation of a transition from shallow to deep cumulus convection. *J. Atmos. Sci.*, **63**, 1895–1909.

Pauluis, O., A. Czaja, and R. Korty, 2008: The global atmospheric circulation on moist isentropes. *Science*, **321 (5892)**, 1075–1078, doi:10.1126/science.1159649.

Pauluis, O., A. Czaja, and R. Korty, 2010: The global atmospheric circulation in moist isentropic coordinates. *J. Climate*, **23**, 3077–3093.

Pauluis, O. M., T. Shaw, and F. Laliberte, 2011: A statistical generalization of the transformed eulerian-mean circulation for an arbitrary vertical coordinate system. *J. Atmos. Sci.*, **68**, 1766–1783.

Romps, D. M. and Z. Kuang, 2010: Do undiluted convective plumes exist in the upper tropical troposphere? *J. Atmos. Sci.*, **67**, 468–484.

Stevens, B., 2005: Atmospheric moist convection. *Annu. Rev. Earth. Planet. Sci.*, **33**, 605–643.

List of Figures

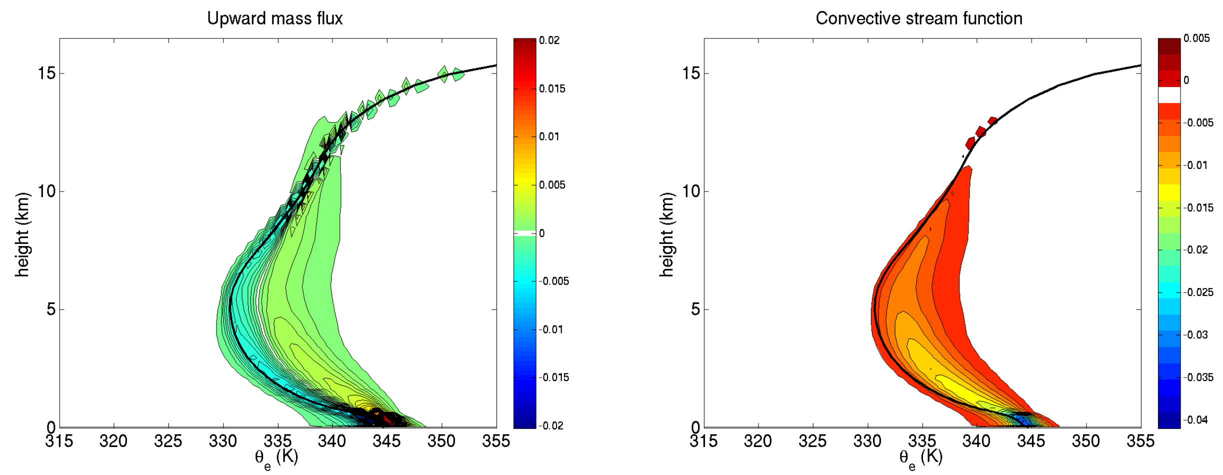

FIG. 1. Left panel: Upward mass flux distribution $\langle \rho w \rangle$ in the radiative-convective equilibrium. Right panel: Isentropic stream function $\Psi(z, \theta_e)$. The solid line shows the mean profile of equivalent potential temperature $\overline{\theta}_e(z)$.

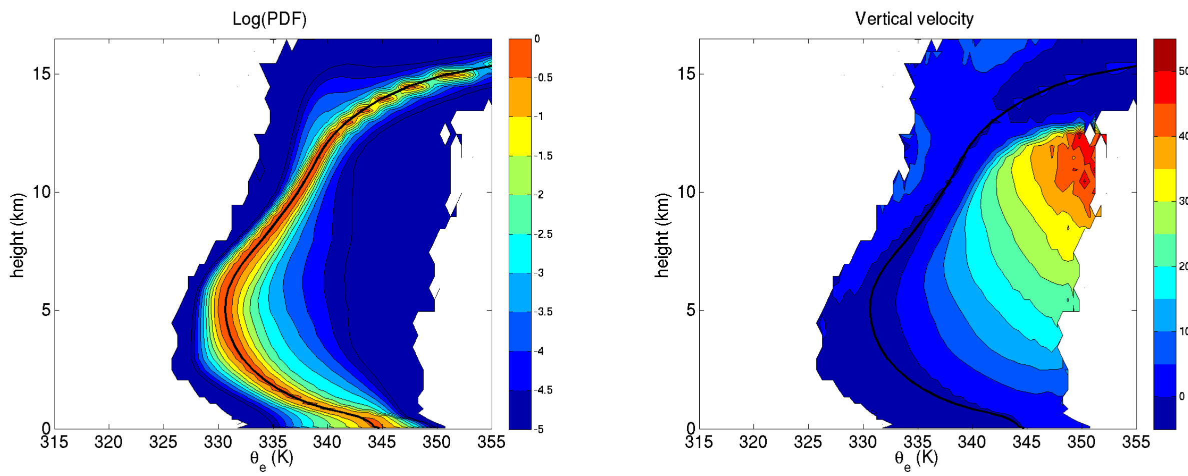

FIG. 2. Left panel: Logarithm of the probability density function for air parcels $f = \langle \rho \rangle / \overline{\rho}(z)$. Right panel: First moment of the vertical velocity $w_1 = \langle \rho w \rangle / \langle \rho \rangle$.

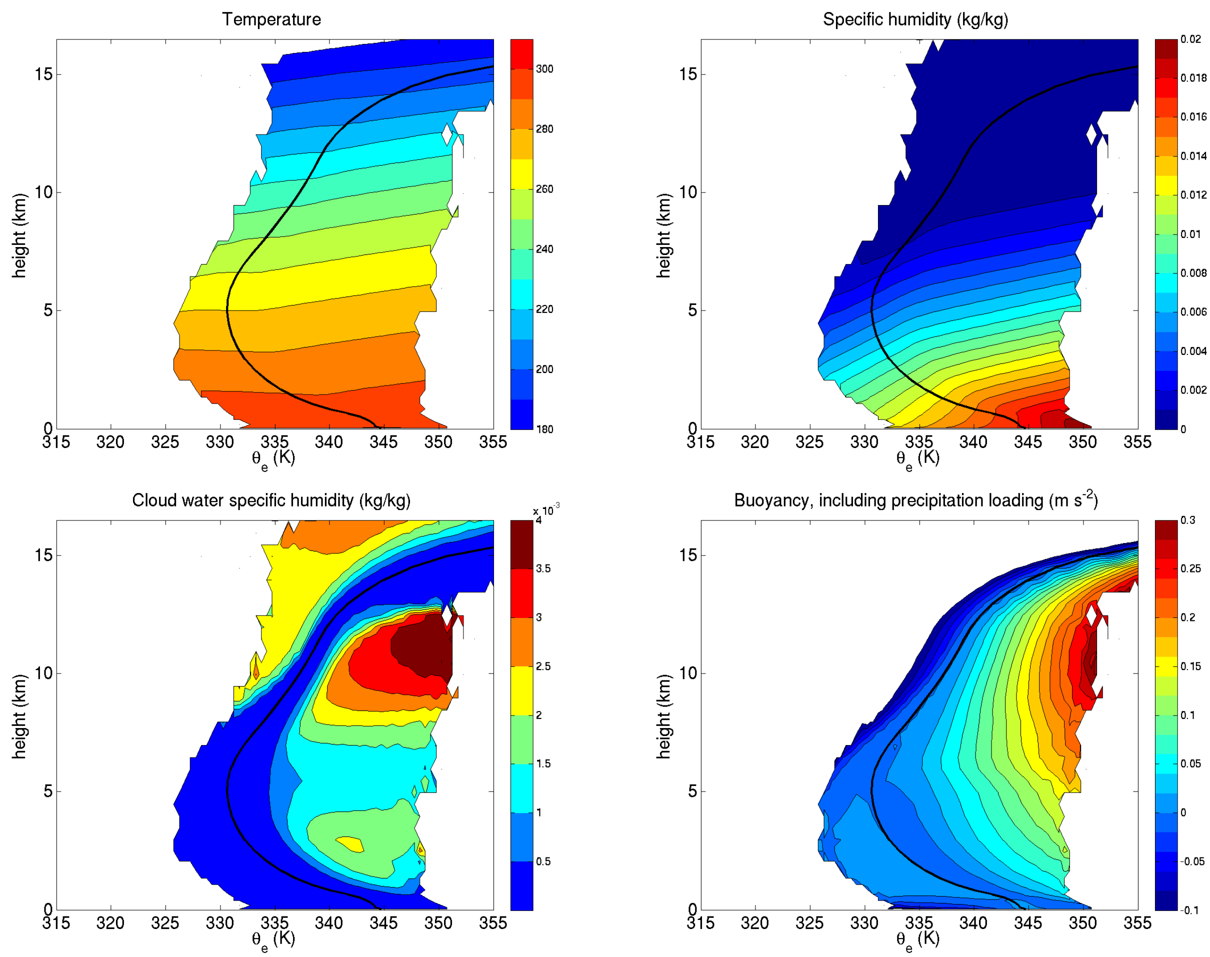

FIG. 3. Upper left panel: First moment of temperature distribution T_1. Upper right panel: First moment of the water vapor distribution q_1. Lower left panel: First moment of the condensed water distribution q_{l1}. Lower right panel: first moment of the buoyancy distribution B_1. See text for definitions.

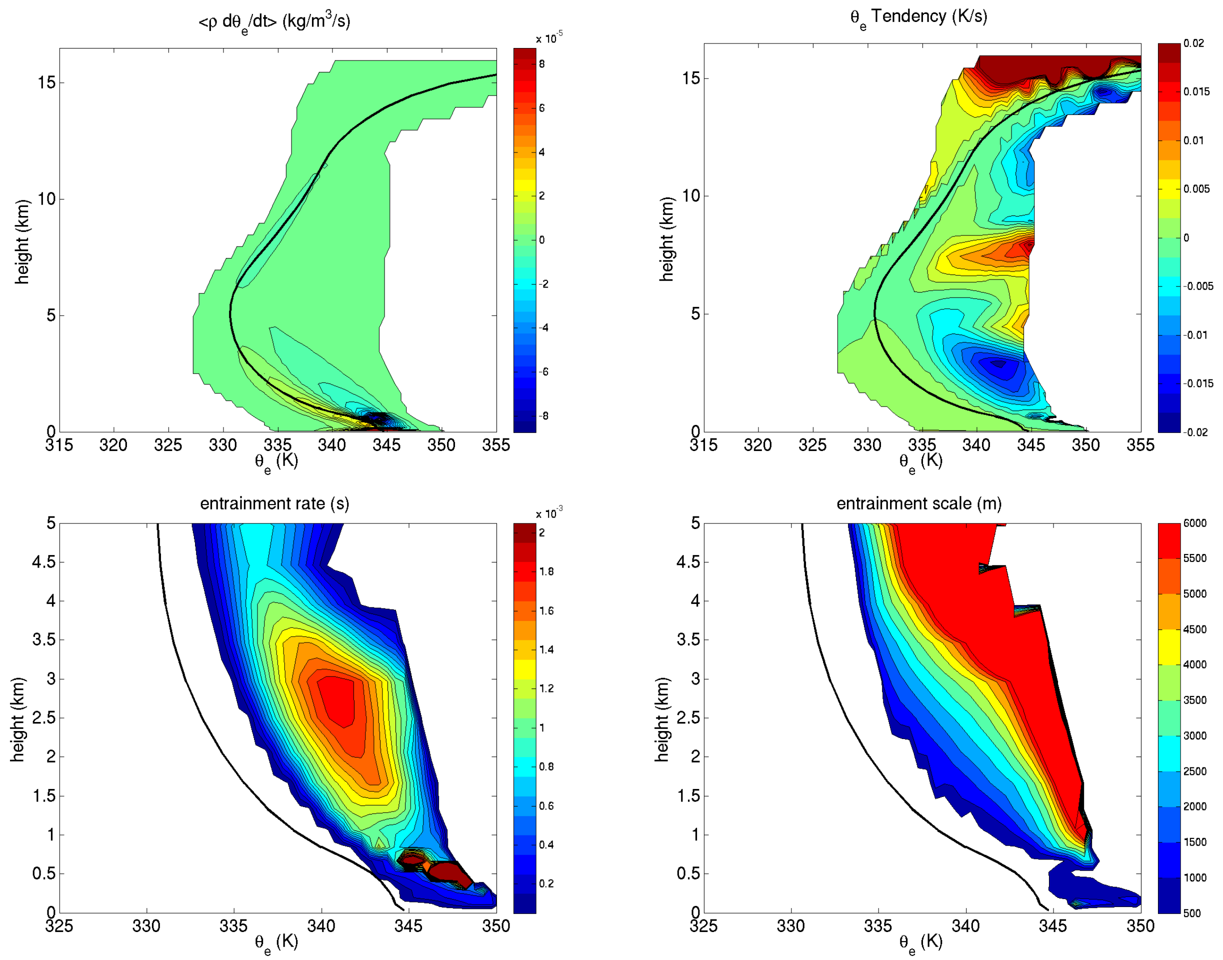

FIG. 4. Upper left panel: Mass weighted diabatic heating $\left\langle \rho\dot{\theta}_e \right\rangle$. Upper right panel: diabatic heating tendency $\tilde{\dot{\theta}}_e$. Lower left panel: Entrainement time-scale from eq. 10. Lower right panel: entrainment scale height from eq. 9

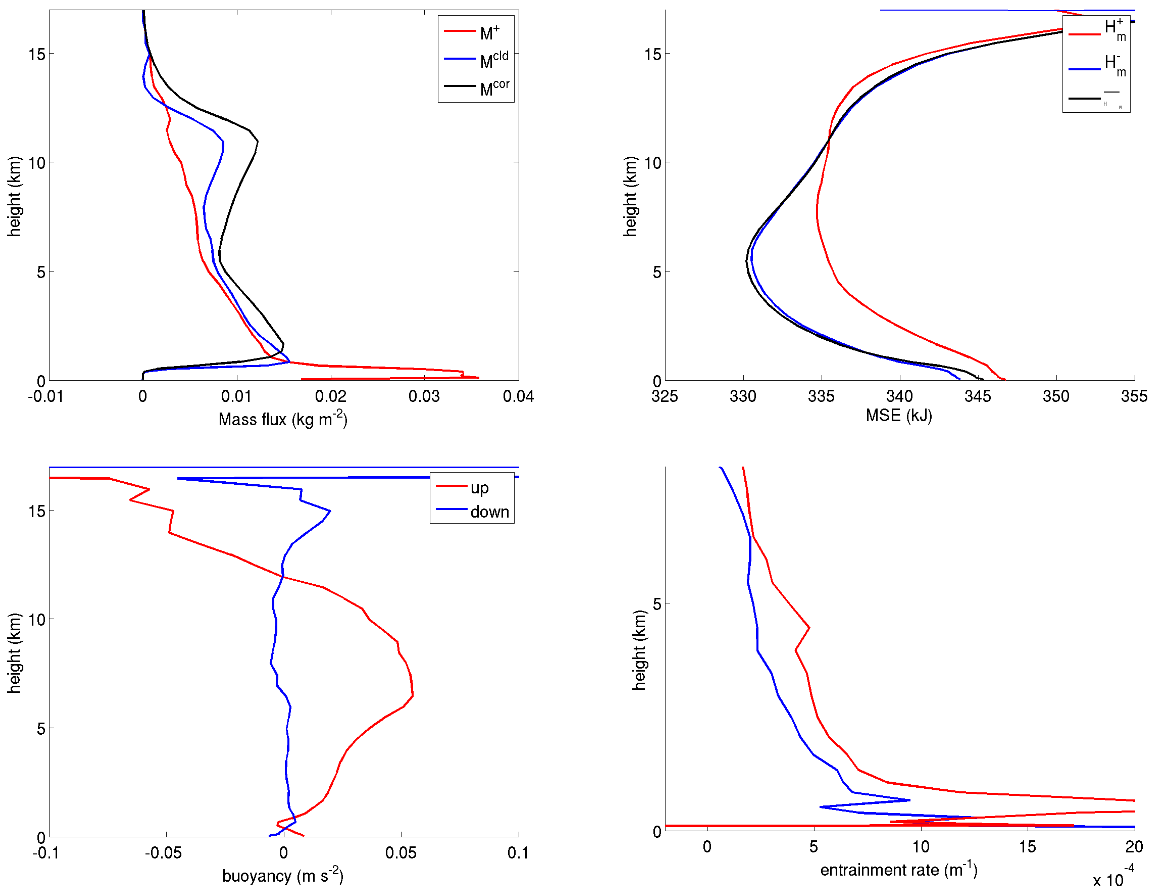

FIG. 5. Results from the two-stream diagnostic for the convection. Upper left panel: upward convective mass flux M^+ from the two stream approximation (solid red line), cloud mass flux ((solid blue line) and mass flux within the convective core (solid black line). Upper right panel: moist static energy in the updraft H_m^+, in the downdraft H_m^- and horizontal mean value $\overline{MSE}$. Lower left panel: buoyancy in the updraft B^+ and in the downdraft B^-. Lower right panel: Entrainment and detrainment rate based on equations (20-21).